Symplectic and antiplectic waves in an array of beating cilia attached to a closed body

Aref Ghorbani[1] and Ali Najafi[1,2,*]
[1]*Department of Physics, Institute for Advanced Studies in Basic Sciences (IASBS), Zanjan 45137-66731, Iran*
[2]*Department of Physics, University of Zanjan, Zanjan 313, Iran*
(Received 28 November 2016; published 22 May 2017)

By taking into account the hydrodynamic interactions in a one dimensional array of model cilia attached to a no-slip cylinderical surface, we investigate their synchronized motion. We show how the emergence of metachronal waves depends on the initial state of the system and investigate the conditions under which the formation of symplectic and antiplectic waves are possible.

DOI: 10.1103/PhysRevE.95.052412

I. INTRODUCTION

Cillium is a micron scale flexible hairlike appendix, and its ensembles appear in many biological systems [1]. Mucociliary transport in the respiratory system and the swimming of ciliated organisms, such as *Volvox* and *Paramecium* are among the most important examples of cilia in biology [2–6]. Using the forces from molecular motor proteins embedded in its molecular structure, an individual cilium can beat and produce a flow field [7]. In most of their natural appearances, the emergent synchronized motion in the form of a metachronal wave developed in assemblies of cilia is an essential key in their performances. This is due to the fact that the flow field corresponding to an individual cilium is negligibly small but a synchronized pattern of ciliary beating is able to either produce a net flow of fluid in mucus or generate a swimming mechanism for the ciliated microorganisms. The metachronal wave is a kind of synchronized pattern of ciliary beating that results in a traveling wave on the envelop of their tips. Experimental studies show that the direction of a metachronal wave can be either parallel (symplectic wave) or antiparallel (antiplectic wave) to the direction of the power stroke in an individual cilium [5,8]. The physical mechanism behind this wave pattern formation is not completely understood, but it is mainly believed that the hydrodynamic interactions between cilia can lead their assembly to reach a synchronized state with propagating metachronal waves [9–11]. There are some experimental observations in artificial active colloidal systems that support the idea of hydrodynamic mediated synchronization in colloidal systems [12–15]. In addition to the hydrodynamic interactions, new studies have suggested that precise coordination of flagellar motion is provided by contractile fibers of the basal membrane [16]. In most recent works a flat geometry for the basal ciliated membrane has been considered [17–23]. Motivated from the hydrodynamic effects due to a rough wall [24], one can expect to see the effects due to the curvature of a ciliated body in the synchronization of its cilia. In a very recent study, the synchronization of cilia attached to a sphere has been addressed, and it is shown that metachronal waves can appear [25]. In this article we revisit the emergence of metachronal waves on a curved ciliated body and consider a ring of cilia attached to the peripheral of a cylindrically curved body. Following the model of Vilfan and Jülicher, we consider each cilium as a small sphere moving along an elliptic trajectory [17]. To take into account the effect of curvature in the hydrodynamic interaction, we use an approximate scheme and assume that the interaction of two adjacent cilia can be calculated using a flat wall that is locally tangent to the surface. We will show that, as a result of asymmetry in the orbit, both symplectic and antiplectic waves can emerge.

II. MODEL

In order to study the motion of an assembly of cilia, we start by defining our simplified mechanical model for a single cilium. To simplify the motion, instead of considering the dynamics of a real cilium which has many degrees of freedom, we can consider the motion of its center of mass. Fluid flow produced by a small sphere located at the position of the center of mass resembles the flow pattern due to the cilium. Regarding the periodic motion of a cilium, the sphere should move on a closed trajectory. Figure 1 (left) mimics the trajectory on which the cilium center of mass moves. Verified by experiments, the ciliary cycle is asymmetric, so the friction forces are different for the first and second halves of the cycle. These half cycles compose the power stroke and the recovery. This asymmetry that should be reflected in the trajectory is essential in allowing the cilium to produce a net flow of fluid along its stroke direction. In determining the dynamics and the shape of the trajectory, one should consider the experimental fact that a cilium has a self sustained dynamics. As a result of this self sustained motion the phase variable, the angle of the motion along the trajectory, is free. This phase freedom is essential in the synchronization of two cilia. Considering this phase freedom, two classes of models can be considered. In the first class of models it is assumed that the trajectory is on average a circular path. This means that the internal forces of molecular motors can be divided into two parts: a constant tangential force along the preferred trajectory and an elastic radial restoring force that guarantees an average finite radius for the trajectory [25,26]. Such a radial elastic force allows the system to behave like a phase-free rotator.

In the second class of models, instead of fixing a value for the tangential force, its response function, a relation between the force and the velocity, has been considered. In this article, we will use this kind of modeling to consider the dynamics of cilia [17,27]. A schematic of the model and its geometrical parameters are shown in Fig. 1 (left). In a reference frame

*najafi@iasbs.ac.ir

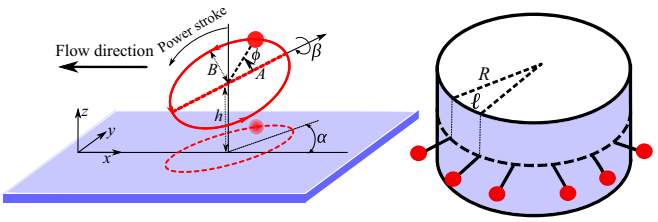

FIG. 1. Left: geometry of a single cilium and right: an array of cilia attached to the surface of a cylinder. The direction of the power stroke and the average flow are shown in the figure.

located on the wall (laboratory frame), the sphere moves on an elliptic orbit that is characterized by six parameters A, B, h, x, α, and β. The lengths of the semimajor and semiminor axes are denoted by A and B, and the position vector of the center of the ellipse is given by $(x,0,h)$. A rigid wall that stands for the body is placed at $z = 0$. The plane of the ellipse and the rigid wall are not parallel; the plane of the ellipse is rotated with an angle β around its semimajor axis. Projecting the orbit on the plane, the semimajor axis is tilted with an angle α with respect to the x axis. For later use we denote the eccentricity of the orbit by $e = \sqrt{1-(\frac{B}{A})^2}$. The instantaneous dynamical state of the sphere moving on this orbit is denoted by an angle $\phi(t)$. In the laboratory frame, the instantaneous position vector for a cilium that depends on time only through the phase variable $\phi(t)$ can be written as

$$\mathbf{r}[\phi(t)] = \begin{bmatrix} x \\ 0 \\ h \end{bmatrix} + \mathcal{R}_A(\beta)\mathcal{R}_z(\alpha) \begin{bmatrix} A\cos\phi \\ B\sin\phi \\ 0 \end{bmatrix},$$

where $\mathcal{R}_z(\alpha)$ and $\mathcal{R}_A(\beta)$ denote the rotation matrices around z and the major axis of the ellipse. In this article we use columnar matrices to show the vectors.

Based on an intuitional argument, we easily can distinguish the direction of average flow produced by a cilium. It is essential to note that only a tilted elliptic trajectory ($\beta \neq 0$) is able to produce net flow. For a tilted trajectory, we can decompose the ciliary cycle into two subtrajectories both parallel to the wall, one near and the other far from the wall. The cilium has more or less the same velocity in both parts, but the friction coefficient is greater in the near wall case. As a result of a smaller friction coefficient, the force exerted on the fluid is stronger at the part that is far from the wall. This means that the motion of a cilium in a part of its trajectory that is far from the wall determines the flow direction. Thus the flow pattern is in the same direction as the cilium moves in its motion where it is far from the wall. For a typical trajectory shown in Fig. 1 (left), the direction of the flow points from right to left. In this argument we have neglected the parts of the trajectory that are perpendicular to the wall, and such parts will have a contribution in flow perpendicular to the wall. In the case of many coordinated cilia, the perpendicular part of the velocity profile averages to zero.

In this article we aim to investigate the curvature of the ciliated body and its role in the dynamic of cilia. In order to attack this problem, we consider a one dimensional array of $\mathcal{N}$ cilia attached to a circle around the cylinder. The circle is wrapped around the cylinder, and it has the same radius R as a cylinder. As shown in Fig. 1 (right), two adjacent cilia are connected with an arc length $\ell = 2\pi R/\mathcal{N}$. The geometrical parameters of each cilium can be expressed with respect to a flat wall that is locally tangent to the cylinder. In the case that the length of each cilium is comparable with this arc length, we expect to see hydrodynamical effects due to the curvature of the body. In the next section we will summarize all of the equations that are necessary to describe the dynamics of a coupled system of cilia.

III. DYNAMICAL EQUATIONS

Let us consider two cilia, each represented by a moving sphere with radii a and position vectors given by $\mathbf{r}_i$ ($i = 1,2$) and corresponding parameters for their elliptic trajectories. Hereafter we consider similar cilia that have the same geometrical and dynamical properties. On the micrometer scale where the dissipative effects dominate over inertial effects, the governing equations for two interacting colloidal particles (here two cilia) can be written as linear relations between the ith particle's velocity $\mathbf{v}_i = \dot{\mathbf{r}}_i$ and the hydrodynamic forces acting on particles denoted by $\mathbf{f}_j$. In terms of their Cartesian components, we have as follows:

$$v_{i,\mu} = \sum_{\nu=1}^{3}\sum_{j=1}^{2} G_{\mu\nu}(\mathbf{r}_i,\mathbf{r}_j) f_{j,\nu}, \tag{1}$$

where the greek letters denote the Cartesian components of the vectors. The hydrodynamic kernel $G_{\mu\nu}$ contains information about the geometry of the system: radii of the spheres, their separation, and their distances to the wall. Assuming that the sphere radius a is much smaller than all other lengths in the system, we can write an approximate form for the component of the hydrodynamic kernel in a semi-infinite domain confined by a rigid wall. For $\mathbf{r}_i \neq \mathbf{r}_j$, we have [28] as follows:

$$G(\mathbf{r}_i,\mathbf{r}_i) \simeq \frac{3}{2\pi\eta}\frac{z_i z_j}{d^3}\begin{pmatrix} \cos^2\psi & \sin\psi\cos\psi & 0 \\ \sin\psi\cos\psi & \sin^2\psi & 0 \\ 0 & 0 & 0 \end{pmatrix}, \tag{2}$$

where η is the fluid viscosity, $z_i = \hat{z}_i \cdot \mathbf{r}_i$, $d = \sqrt{(x_j-x_i)^2+(y_j-y_i)^2}$, and we have assumed that $z_i, z_j \ll d$. Here ψ is defined as $\tan\psi = (y_j-y_i)/(x_j-x_i)$. For $\mathbf{r}_i = \mathbf{r}_j$, we have as follows:

$$G(\mathbf{r}_i,\mathbf{r}_i) \simeq \frac{1}{6\pi\eta a}\begin{pmatrix} 1-\epsilon & 0 & 0 \\ 0 & 1-\epsilon & 0 \\ 0 & 0 & 1-2\epsilon \end{pmatrix}, \tag{3}$$

where $\epsilon = (9a/16z)$. Let us continue our discussion about the case of two interacting cilia near a flat wall, then we will discuss how the effects due to the curvature of the body can be considered. Denoting the inverse of hydrodynamic kernel $G(\mathbf{r}_j - \mathbf{r}_j)$ by matrices M_{ij}, the hydrodynamic equations can be rewritten as

$$\begin{aligned} \mathbf{f}_1 &= M_{11}\mathbf{v}_1 + M_{12}\mathbf{v}_2, \\ \mathbf{f}_2 &= M_{21}\mathbf{v}_1 + M_{22}\mathbf{v}_2. \end{aligned} \tag{4}$$

In addition to the above hydrodynamic equations, we should provide some information about the internal forces inside each

cilium that drive its beating. In addition to constraining forces that enforce the particle to move on an elliptical orbit, there is also a tangential force that results the motion along orbit. Denoting the unit vector tangent to the trajectory of the ith cilium by $\mathbf{t}_i = \frac{d}{d\phi_i}\mathbf{r}_i$, the velocity can be written as $\mathbf{v}_i = \dot{\phi}_i \mathbf{t}_i$. The tangential component of the force reads as $f_i^t = \hat{\mathbf{t}}_i^T \mathbf{f}_i$, where the symbol T denotes the transpose of a columnar matrix and we use matrix multiplication rules. In general, the tangential force is related to the velocity of the sphere along its trajectory given by $v_i^t = \hat{\mathbf{t}}_i \cdot \mathbf{v}_i$. In the linear response regime, equations, such as

$$\mathbf{t}_i^T \mathbf{f}_i = f_0\big(1 - v_0^{-1}|\mathbf{t}_i|\dot{\phi}_i\big) \tag{5}$$

capture the dynamics of the ith cilium. Here f_0 is the stall force, and it is the amount of external force necessary to stop the motion of a beating cilium. A free cilium that is not affected by any external force moves with velocity v_0. In this linear response approximation, two parameters f_0 and v_0 are related to the microscopic details of the cilium. For a typical cilium, $f_0 \sim 10$ pN, $a \sim 10$ μm, and $v_0 \sim 100$ $\mu\mathrm{m\,s}^{-1}$ [29,30]. Using these numerical values, one can have an estimate for the stiffness of the cilium that is defined by $\kappa = f_0/6\pi\eta a v_0 \sim 1$. This stiffness is the only dimensionless parameter that determines the state of motion for a cilium.

Using Eqs. (4) and (5), we can arrive at the following coupled equations for the phase variables:

$$\dot{\phi}_1\big[\mathbf{t}_1^T M_{11}\mathbf{t}_1 + (f_0/v_0)|\mathbf{t}_1|\big] + \dot{\phi}_2 \mathbf{t}_1^T M_{12}\mathbf{t}_2 = f_0,$$
$$\dot{\phi}_1 \mathbf{t}_2^T M_{21}\mathbf{t}_1 + \dot{\phi}_2\big[\mathbf{t}_2^T M_{22}\mathbf{t}_2 + (f_0/v_0)|\mathbf{t}_2|\big] = f_0.$$

Solving these equations, one can reach equations that reveal the dynamics of phases for the two cilia case.

Let us now explain how can we take into account the curvature effects. In order to study the curvature, the hydrodynamic kernel should be replaced. In a confined space that is limited by a curved wall, the above mentioned kernel G and subsequently its inverse given by matrix M are no longer valid. We proceed by an approximate scheme to consider the curvature effects. Here we assume that, for two interacting cilia, there is an effective plane that can be used for constructing the image system. This effective wall is a wall that is locally tangent to the curved body at the midpoint of two cilia. We can use the results of flat-wall confinement to obtain the approximate interaction between two adjacent cilia. It is obvious that, with this approximation, we do not expect to see any curvature effect in the motion of two cilia. This approximation can only include nontrivial curvature effects to the motion of many cilia (more than two) attached to the cylinder, and it allows us to develop a consistent way for applying the closed boundary condition. This approximation is valid for the case where the radius of curvature is larger than all other length scales in the system, namely, $R \gg \ell$ and $R \gg h$.

To obtain the dynamics of two coupled cilia, one should note that, in a way that we have parametrized the orbits, the kinematics of each cilium can be expressed by a single phase denoted by $\phi_i(t)$. This phase variable is shown in Fig. 1. Solving the dynamical equations and applying the geometrical and dynamical constraints, we will arrive at the following equation [17]:

$$\dot{\phi}_i(t) = g_1(\phi_i)\omega_0 + g_2(\phi_i, \phi_j). \tag{6}$$

Here $\omega_0 = f_0/[6\pi\eta a B(1+\kappa)]$, and the interactions between cilia are reflected by function g_2 that couples the dynamics of the phases. It is not possible to present analytical closed relations for functions g_1 and g_2, but, in principle, we are able to evaluate and study them numerically. In the next section, we will summarize the results of numerical investigations of the above equation.

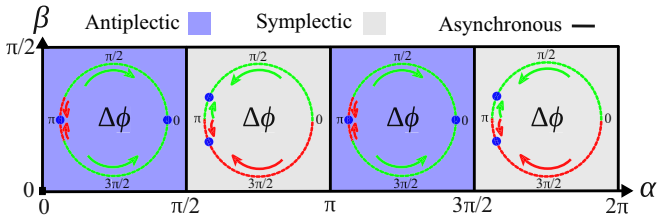

FIG. 2. Phase diagram for the state of synchronization for two or many cilia. Synchronization of two cilia depends on initial phase differences $\Delta\phi(0)$ and α. Different values of $\Delta\phi(0)$ are shown by points on a unit circle. The synchronized states of two cilia are represented by the long time value of their phase differences $\Delta\phi(\infty)$ and are shown by bold dots on the circles. The arrows show the direction of the phase evolution from the initial values toward their final synchronized state, and different colors are used to show the evolution to different final states. For many cilia, both symplectic and antiplectic waves can emerge. For any $\beta \neq 0$, antiplectic (symplectic) waves emerge for $0 < \alpha < \pi/2$ and $\pi < \alpha < 3\pi/2$ ($\pi/2 < \alpha < \pi$ and $3\pi/2 < \alpha < 2\pi$). Numerical parameters are as follows: $a/h = 0.2$, $h/\ell = 0.19$, $B/\ell = 0.19$, $\beta = \pi/4$, and $e = 0.87$.

IV. RESULTS AND DISCUSSION

Before studying the wave propagation in a ciliated curved body, we consider the dynamics of two coupled cilia. Recalling the geometry of elliptic orbits, angles α and β play an important role in the dynamics of coupled cilia. Numerical solutions to the equations for two interacting cilia show that, for $\beta = 0$ and $\beta = \pi/2$ (orbits are parallel and perpendicular, respectively, to the wall), the long time dynamics of cilia does not show any correlations in their beating patterns. In this case, the hydrodynamic mediated interactions between two cilia act in an incoherent way, and the state of motion for each cilium is independent of the other. This result is consistent with previous works of beating cilia near a flat wall [26,31]. When elliptic orbits are tilted ($\beta \neq 0, \pi/2$), temporal correlations in the long time dynamics of interacting cilia will appear. Our numerical studies show that, for tilted orbits, the cilia reach a phase-locked synchronized state. At this synchronized state, the phase difference $\Delta\phi(t) = \phi_2(t) - \phi_1(t)$ reaches a constant value that we will denote by $\Delta\phi(\infty)$. The steady state phase difference $\Delta\phi(\infty)$ depends on initial conditions, the angle of ellipses α and e. Figure 2 shows the state of synchronization and its dependence on α, β, and $\Delta\phi(0)$ for $e \neq 0 (= 0.87)$. As one can see from this figure, for $0 < \alpha < \pi/2$ and $\pi < \alpha < 3\pi/2$, depending on the initial phase difference between cilia, the final state can be either $\Delta\phi(\infty) = 0$ or $\Delta\phi(\infty) = \pi$. The behavior for other values of α and its sensitivity to the initial

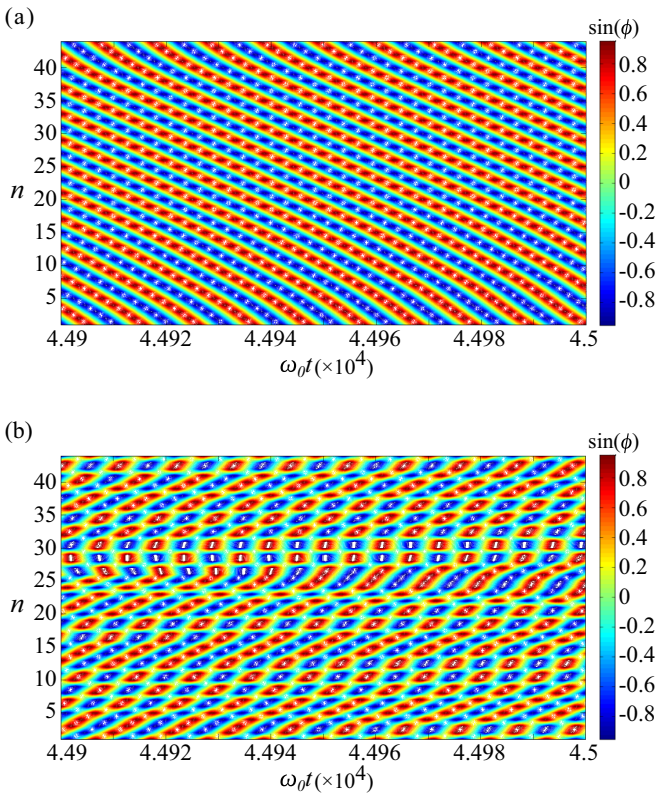

FIG. 3. The state of synchronization in a collection of cilia can be seen in a time-phase portrait. The vertical axes show the cilium number n, the horizontal axes show the time and the value of $\sin[\phi_n(t)]$ are encoded via colors. A symplectic wave appears for (a) $\alpha = 2\pi - \frac{\pi}{4}$, and an antiplectic wave appears for (b) $\alpha = \frac{\pi}{4}$. The numerical parameters are $a/h = 0.2$, $h/\ell = 0.35$, $B/\ell = 0.22$, $e = 0.87$, and $\beta = \pi/4$.

phase difference can be seen in the figure. For $\pi/2 < \alpha < \pi$ and $3\pi/2 < \alpha < 2\pi$, $\Delta\phi(\infty)$ approaches a constant value $\pi + \delta$ where, depending on the initial phase difference, δ could also be a positive or negative small angle. Angle δ depends on α, and as an example, for $\alpha = -\pi/4$, it reaches $\pi/6$. The synchronization picture shown in Fig. 2 is valid for any $e \neq 0$. For a special case of $e = 0$ where the orbits are circular and for $0 < \alpha < \pi/2$ and $\pi < \alpha < 3\pi/2$, we observed that the two cilia system reaches a synchronized state with $\Delta\phi(\infty) = 0$. When $e = 0$ and for $\pi/2 < \alpha < \pi$ and $3\pi/2 < \alpha < 2\pi$, the systems reach a state with $\Delta\phi(\infty) = \pi$.

Let us examine the dynamics of a one dimensional array of $\mathcal{N} = 44$ cilia, attached to the circumference of a cylinder. We took into account the hydrodynamic interactions and considered both cases of elliptic and circular orbits separately ($e = 0$ and $e = 0.87$). Interestingly, unlike the case of two cilia, the emergence of synchronized states does not show any dependence on the value of e. Figure 3 shows two examples for the time evolution of the phase variables for all cilia. The phase values are encoded via colors. The patterns shown in this figure demonstrate the long time dynamics of the system. The regularity of the long time patterns reflects the temporal correlations in the motion of the cilia. In this case, a traveling metachronal wave shows a synchronized state of the cilia [9,30,31]. For a propagating wave (metachronal wave) in the array of the cilia, the phase of the nth cilium $\phi_n(t)$ can be written as $\phi_n(t) = nK - \Omega t$ where the number K plays the role of a wave number associated with a metachronal wave. In the regular patterns shown in Fig. 3, the regions with constant phases (same colors) make straight lines. These straight lines are given by an equation, such as $nK = \Omega t + C$, where C is a constant. The slope of these parallel lines measures the wavelength of a metachronal wave, and it is given by $1/K = \partial n/\partial(\Omega t)$. For $K > 0$, the wave moves in a direction with the increasing cilium's number n. As shown in Fig. 1, the flow direction always points to the left (from large n to small n cilia). So we conclude that a positive slope corresponds to antiplectic and a negative slope shows a symplectic metachronal wave. Figure 3 shows two examples of metachronal waves for $\alpha = \pi/4$ and $\alpha = 2\pi - \pi/4$. As one can see, in the first case [Fig. 3 (up)], a symplectic wave has appeared, and for the second case [Fig. 3 (down)], an antiplectic wave has appeared. The results of our numerical investigations for the synchronization of an ensemble of cilia are shown in Fig. 2. The results show that the emergence of such synchronized states (simplectic and antiplectic) crucially depends on the value of α. Independent of the value of e, the antiplectic metachronal waves appear for $0 < \alpha < \pi/2$ and $\pi < \alpha < 3\pi/2$. On the other hand, symplectic metachronal waves appear when $\pi/2 < \alpha < \pi$ and $3\pi/2 < \alpha < 2\pi$. Changing α to $2\pi - \alpha$, the average direction of the fluid flow does not change, but the propagation direction of the metachronal wave will change. Comparing the results for an array of cilia with the results of two cilia, one can see that the emergence of symplectic or antiplectic synchronization in an array of cilia is related directly to the state of synchronization in the case of two cilia. It is interesting that the antipletic waves accompany many defects in their structures. Such defected waves have been seen in a chain of model cilia [14].

In conclusion, the state of synchronization is studied for interacting cilia. For two cilia, the synchronized state depends on the initial phase difference and the geometrical parameters of the trajectories given by α and β. In-phase antiphase ($\delta\phi = 0,\pi$) synchronized states have been observed. For a $1 - D$ array of cilia attached to a curved body, we found that both symplectic and antiplectic metachronal waves can appear. The emergence of symplectic and antiplectic waves in an array of cilia is in direct connection with the state of synchronization in the two cilia case. As a result of our paper, we understand the geometrical characteristics are key elements in determining the state of metachronal waves. The emergence of a symplectic or antiplectic metachronism in our model is not an artifact of imposing a closed boundary condition. The boundary condition in our system emerges naturally from the closed structure of the curved body.

[1] B. Alberts, A. Johnson, J. Lewis, K. Roberts, M. Raff, and P. Walter, *Molecular Biology of the Cell* (Garland Science, New York, 2002).

[2] J. Blake, J. Fluid Mech. **46**, 199 (1971).

[3] A. Dummer, C. Poelma, M. C. DeRuiter, M.-J. T. Goumans, and B. P. Hierck, Cilia **5**, 1 (2016).

[4] D. B. Hill, V. Swaminathan, A. Estes, J. Cribb, E. T. O'Brien, C. W. Davis, and R. Superfine, Biophys. J. **98**, 57 (2010).
[5] *Biocommunication of Ciliates*, edited by G. Witzany and M. Nowacki (Springer, Basel, 2016).
[6] C. Brennen and H. Winet, Annu. Rev. Fluid Mech. **9**, 339 (1977).
[7] I. H. Riedel-Kruse, A. Hilfinger, J. Howard, and F. Jülicher, HFSP J. **1**, 192 (2007).
[8] E. W. Knight-Jones, J. Cell Sci. **3**, 503 (1954).
[9] S. Gueron and K. Levit-Gurevich, Biophys. J. **74**, 1658 (1998).
[10] M. Lighthill, Commun. Pure Appl. Math. **5**, 109 (1952).
[11] A. Najafi and R. Golestanian, Europhys. Lett. **90**, 68003 (2010).
[12] J. Kotar, M. Leoni, B. Bassetti, M. C. Lagomarsino, and P. Cicuta, Proc. Natl. Acad. Sci. USA **107**, 7669 (2010).
[13] R. D. Leonardo, A. Búzás, L. Kelemen, G. Vizsnyiczai, L. Oroszi, and P. Ormos, Phys. Rev. Lett. **109**, 034104 (2012).
[14] D. R. Brumley, N. Bruot, J. Kotar, R. E. Goldstein, P. Cicuta, and M. Polin, Phys. Rev. Fluids **1**, 081201 (2016).
[15] D. R. Brumley, K. Y. Wan, M. Polin, and R. E. Goldstein, Elife **3**, e02750 (2014).
[16] K. Y. Wan and R. E. Goldstein, Proc. Natl. Acad. Sci. USA **113**, E2784 (2016).
[17] A. Vilfan and F. Jülicher, Phys. Rev. Lett. **96**, 058102 (2006).
[18] N. Uchida and R. Golestanian, Phys. Rev. Lett. **106**, 058104 (2011).
[19] H. Stark and M. Reichert, J. Biomech. **39**, S349 (2006).
[20] J. Elgeti and G. Gompper, Proc. Natl. Acad. Sci. USA **110**, 4470 (2013).
[21] D. R. Brumley, M. Polin, T. J. Pedley, and R. E. Goldstein, J. R. Soc., Interface **12**, 20141358 (2015).
[22] B. Qian, H. Jiang, D. A. Gagnon, K. S. Breuer, and T. R. Powers, Phys. Rev. E **80**, 061919 (2009).
[23] R. Golestanian, J. M. Yeomans, and N. Uchida, Soft Matter **7**, 3074 (2011).
[24] S. H. Rad and A. Najafi, Phys. Rev. E **82**, 036305 (2010).
[25] B. Nasouri and G. J. Elfring, Phys. Rev. E **93**, 033111 (2016).
[26] P. Lenz and A. Ryskin, Phys. Biol. **3**, 285 (2006).
[27] B. Guirao and J.-F. Joanny, Biophys. J. **92**, 1900 (2007).
[28] C. Pozrikidis, *Boundary Integral and Singularity Methods for Linearized Viscous Flow* (Cambridge University Press, Cambridge, U.K., 1992).
[29] J. Howard, *Mechanics of Motor Proteins and the Cytoskeleton* (Sinauer Associates, Sunderland, MA, 2001).
[30] D. R. Brumley, M. Polin, T. J. Pedley, and R. E. Goldstein, Phys. Rev. Lett. **109**, 268102 (2012).
[31] T. Niedermayer, B. Eckhardt, and P. Lenz, Chaos **18**, 037128 (2008).